Composite Interfaces
Publication details, including instructions for authors and subscription information:
http://www.tandfonline.com/loi/tcoi20

Notch effect in clay-modified epoxy: a new perspective on nanocomposite properties

M. Zappalorto [a], M. Salviato [a], A. Pontefisso [a] & M. Quaresimin [a]
[a] Department of Management and Engineering, University of Padova, Stradella San Nicola 3, Vicenza, 36100, Italy
Published online: 20 Jun 2013.

To cite this article: M. Zappalorto, M. Salviato, A. Pontefisso & M. Quaresimin (2013) Notch effect in clay-modified epoxy: a new perspective on nanocomposite properties, Composite Interfaces, 20:6, 405-419, DOI: 10.1080/15685543.2013.807147

To link to this article: http://dx.doi.org/10.1080/15685543.2013.807147

Composite Interfaces, 2013
Vol. 20, No. 6, 405–419, http://dx.doi.org/10.1080/15685543.2013.807147

Notch effect in clay-modified epoxy: a new perspective on nanocomposite properties

M. Zappalorto, M. Salviato, A. Pontefisso and M. Quaresimin*

Department of Management and Engineering, University of Padova, Stradella San Nicola 3, Vicenza 36100, Italy

(*Received 14 March 2013; accepted 8 May 2013*)

In this work, an experimental investigation of the notch effect on clay-modified epoxy resins is carried out, discussing the results from Single Edge Notch Bending tests and Double Edge Notch Tension tests on notched components. It is found that when the notch root radius is greater than a limit value, which depends on the clay content, the brittle failure of notched nanomodified specimens is controlled by the material strength. Under this circumstance nanomodification, while enhancing the polymer fracture toughness, might have a detrimental effect on the strength of notched components. This study brings to light a new feature of nanomodification according to which particular care should be used when using nanomodified resins for structural applications in the presence of notches or holes.

Keywords: nanocomposites; nanoclay; notch effect; mixed mode

1. Introduction

Nanocomposites are new multifunctional materials endowed with exceptionally improved mechanical and physical properties at very low filler concentrations.[1–3] This behaviour, often regarded as the 'nano-effect', is acknowledged to be due to the molecular structure of the material. Indeed, in the presence of nanofiller-reinforced polymers, the specific surface is extremely large, and this makes surface properties the dominant factor, providing unique properties with widespread applications in many industrial sectors.

Moreover, as the reinforcement size is comparable with that of polymeric chains, molecular interactions with the matrix produce an interphase 'layer' with properties potentially different from those of the constituents. In the recent literature, it has been demonstrated that the properties of the interphase might significantly affect the overall mechanical properties of the nanocomposite depending also on the filler size and geometry.[4–7]

Nanoclays are layered silicates of which the platelets are micro-sized in area, about 1 nm thick and disposed in stacks called tactoids. Once dispersed in the polymeric matrix, three typical nanoclay morphologies are possible, namely, exfoliated, intercalated and phase separated.

Experimental results from the literature reveal that nanoclays are suitable to improve the tensile elastic modulus, the fracture toughness of polymeric systems [8–10] and the

*Corresponding author. Email: marino.quaresimin@unipd.it

fatigue threshold,[11,12] while conflicting results have been reported with reference to the strength of nanoclay reinforced resins, which has been proven either to increase [13,14] or to decrease,[12,14–16] depending on the investigated system.

In the perspective to use nanomodified polymers as toughened matrixes in ternary, fibre reinforced, nanocomposites, the fracture toughness is acknowledged to be the most important mechanical property to be improved.[11,12,17–21] This explains the great efforts dedicated by several researchers to study the fracture toughness of binary nanocomposites (polymer matrix plus nanofillers).[13,22–25] All the above-mentioned works are referred to the pure mode I fracture toughness of nanofilled polymers. Only very recently, inspired by the argument that in practice the stress state ahead of a crack is often of the mixed type, the attention has been moved also onto the mixed mode fracture behaviour of cracked nanoclay/epoxy specimens [26] and nanotubes/epoxy specimens.[27] In particular, Zappalorto et al. [26] found that nanomodified specimens exhibit a higher fracture toughness, independently of the loading mode, but ranging from pure mode I to pure mode II improvements are less pronounced.

Despite the fact that geometrical variations unavoidably exist in engineering components, in the best of the authors' knowledge, the effects of notches on the mechanical behaviour of clay-modified epoxy resins have been completely ignored in the previous literature. With the aim to fill this gap, in this study the brittle notch fracture behaviour of an epoxy resin filled with montmorillonite nanoclays is analysed. To this end, different kind of specimens have been manufactured and tested:

- Double Edge Notch Tension (DENT) specimens with 4 mm radius semicircular notches;
- Single Edge Notch Bending (SENB) specimens with U-notches characterised by three different values for the notch root radius (0.5, 1 and 2 mm).

The effect of nanoclay content on the strength of notched component is discussed in detail. In particular, for the material systems and geometries investigated in this work, nanomodification is found to have a detrimental effect on the strength of notched components. This behaviour is due to the fact that for notch root radii greater than a limit value, which depends on the clay content, the brittle failure of notched nanomodified specimens is a strength-controlled phenomenon. In all these cases, the disadvantageous role played by nanoclay addition on the strength of polymeric resins [12,14–16] is transferred to the notch effect on nanomodified specimens.

This important result makes it evident a new feature of nanocomposites: even if the fracture toughness of nanofilled polymers is generally higher with respect to that of the neat resin, particular care should be taken when using binary nanomodified resins for structural applications in the presence of notches or holes.

A summary of all the experimental results is eventually presented in terms of both the maximum principal stress at the notch edge and the generalised stress intensity factors (GSIFs).

2. Materials and specimens used in the experimental analysis

In this study, a DGEBA-based epoxy resin (EC157 with W152LR hardener) from ELANTAS-Camattini (Italy) is chosen as polymer matrix. The mechanical properties of the epoxy system, as specified by the supplier, are summarised in Table 1.

Table 1. Elastic modulus (E), ultimate strength (σ_R) and fracture strain (ε_R) of EC157/W131 epoxy system as provided by the supplier.

E	3.2 3.5 GPa
σ_R	68–76 MPa
ε_R	6–8%

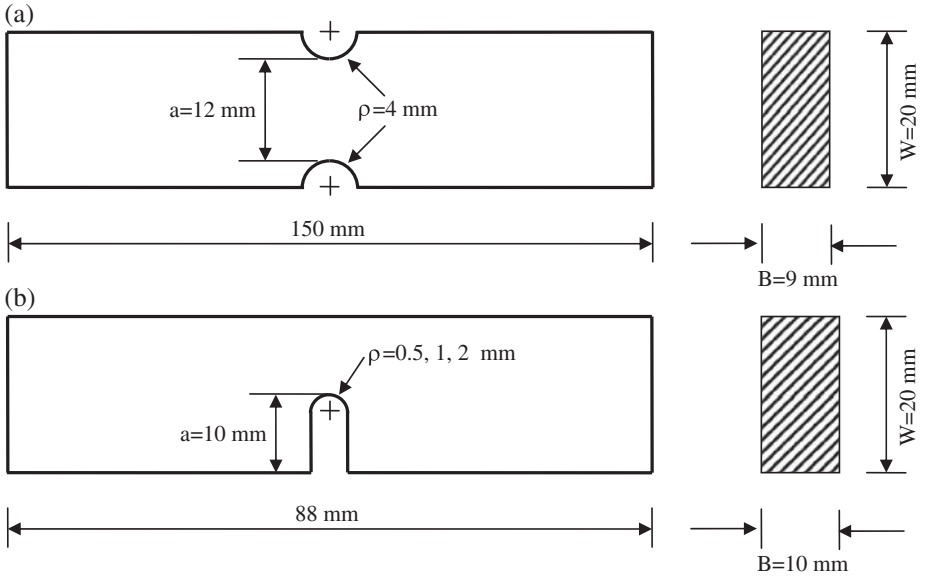

Figure 1. (a) Double Edge Notch Tension (DENT) specimens and (b) Single Edge Notch Bending (SENB) used in the tests.

In addition, a montmorillonite clay, Cloisite 30B® from Southern Clay Products, is used as nanosized reinforcement, considering different weight fractions. 30B nanoclays are characterised by 1 nm thick lamellae, lateral dimensions from 70 to 150 nm and average d-spacing of about 18.5 Å.

Different kind of specimens have been manufactured and tested:

(1) DENT specimens with 4 mm radius semicircular notches (Figure 1(a));
(2) SENB specimens with U-notches. In this case, the notch depth is equal to 10 mm and three different values for the notch root radius have been used: 0.5, 1 and 2 mm (Figure 1(b)).

In the best of authors' knowledge, there is no standard available for fracture tests on notched components. Accordingly, as far as tests on SENB specimens are concerned, the same specimen size and geometry suggested for mode I fracture tests [28] have been used.

The specimens were manufactured according to the following steps:

(1) *Dispersion of the filler within the resin*: Nanoclays were dispersed within the polymer resin through shear mixing followed by sonication. The shear mixing

process was carried out with a DISPERMAT TU shear blender from VMA-Getzmann, at an average rate of 2000 rpm for about 1 h. The sonication process, instead, was performed using a HIELSCHER UP 200s Sonicator, set on 140 W (70% of the maximum power) and a duty cycle of 50%, for 10 min. After sonication, the hardener was added and the obtained blend was mixed at low rate (1000 rpm) for further 5 min.

(2) *Degassing and moulding of the obtained blend*: As a major drawback of the shear mixing process, a large amount of air is trapped into the matrix. Thus, in order to prevent bubbles in the specimens, a careful degassing process was carried out. To this end, a low-vacuum pump was used to induce a very low pressure in the resin pot, promoting bubbles explosion. One hour of degassing process was enough to obtain a clear and translucent nanomodified resin which was later slowly poured into silicone rubber moulds. The different stages of the degassing process are shown in Figure 2.

(3) *Milling and surface polishing*: Once demoulded, the specimens were milled to cut out the upper surface, where some inclusions and voids due to the pouring process could have been present, and polished up to the final thickness.

The morphology of the systems analysed in this work has been investigated using scanning electron microscopy (SEM), in order to identify the presence of nanofiller agglomerates. As an example, Figure 3 shows some SEM images for 3 wt% loaded resins. The filler presents a satisfactory distribution within the matrix but some traces of

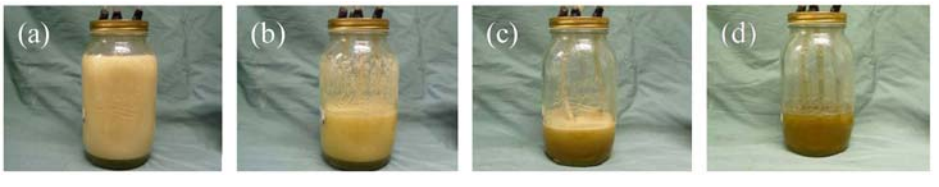

Figure 2. Degassing process of the nanomodified resin (5%wt of nanoclay). (a) Nanomodified resin at low pressure as just poured into the pot; (b) after 10 min; (c) after 25 min and (d) after 35 min. At the end of the process, the mixture is devoid of any bubble.

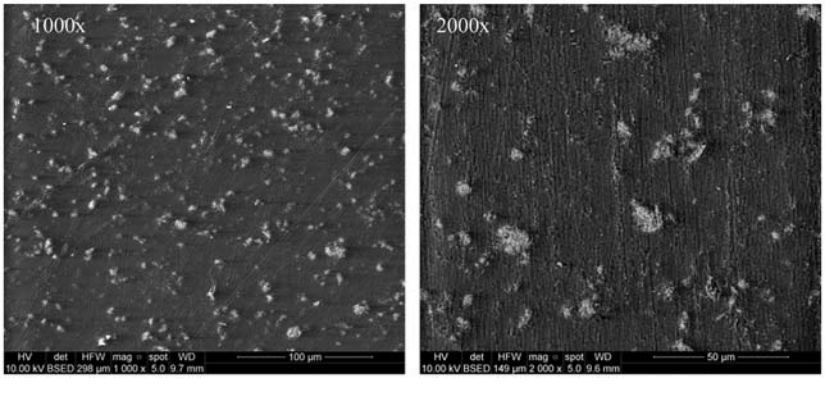

Figure 3. Morphology of 3%wt clay-loaded resins. Scanning electron micrographs at different magnifications.

clay agglomeration are evident, the size of the largest agglomerates among those detected being about 15 μm. A similar morphology was found in Ref. [12]; in that case, an increase of about 35% of the mode fracture toughness was found.

3. Experimental equipment and tests

All tests described in the following have been carried out by using a MTS 858 servo-hydraulic machine, equipped with a 2.5/25 kN load cell.

3.1. DENT tests

Tensile tests on DENT specimens made of neat epoxy and nanomodified resins were carried out, by using a cross-head speed equal to 2 mm/min. For each material configuration, five specimens were tested.

It is worth mentioning here that the theoretical stress concentration factor referred to the net area for the DENT specimens used in the present analysis is equal to 1.866.[29]

3.2. SENB tests

As far as SENB tests are concerned, different loading conditions have been applied, resulting in different stress states ahead of the notch tip, from pure mode I (completely symmetric stress state) to pure mode II (completely skew-symmetric stress state).

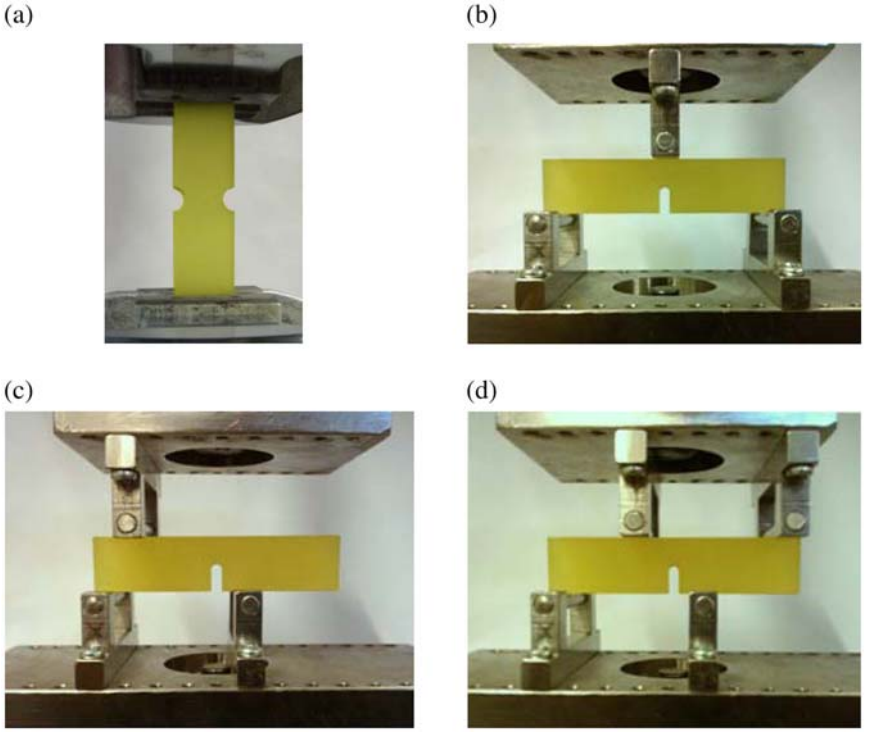

Figure 4. Pictures of the loading configurations for DENT tests (a), Symmetric Three Point Bending (S3 PB) tests (b), Non-Symmetric Three Point Bending (NS3 PB) tests (c) and Non-Symmetric Four Point Bending (NS4 PB) tests (d).

The experimental tests have been carried out using a cross-head speed equal to 10 mm/min, as suggested in [28,30] for cracked components. For every loading condition and every filler weight fraction, three specimens were tested.

The testing device consisted of two steel plates, 18 mm thick, one fixed on the load cell and the other attached to a vertical moving ram. One or two pin support could be mounted on each plate.

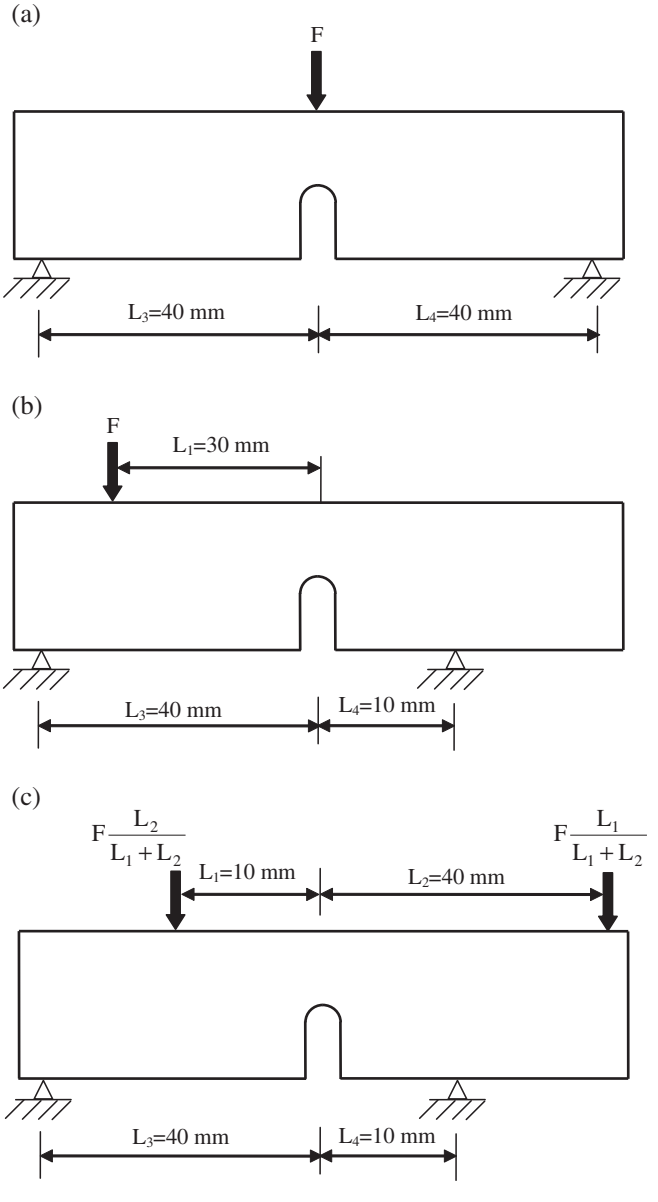

Figure 5. Schematic of the Symmetric Three Point Bending (S3 PB): (a) Non-Symmetric Three Point Bending (NS3 PB) (b) and of the Non-Symmetric Four Point Bending (NS4 PB) (c) loading configurations used in the experimental analyses.

Table 2. Values of stress concentration coefficient K for SENB specimens.

	K		
ρ [mm]	S3 PB	NS3 PB	NS4 PB
0.5	3.436	4.265	6.062
1	2.518	3.165	4.626
2	1.903	2.433	3.696

Three different kind of loading conditions have been analysed;

(1) Symmetric Three-Point Bending tests (S3 PB) which result in a purely symmetric stress state close to the notch tip (pure mode I loading conditions);
(2) Non-Symmetric Three-Point Bending tests (NS3 PB) which result in a mixed (symmetric plus skew-symmetric) stress state close to the notch tip;
(3) Non-Symmetric Four-Point Bending tests (NS4 PB) which result in a purely skew-symmetric stress state close to the notch tip (pure mode II loading conditions).

Some pictures of the loading system are shown in Figure 4, while schematics of the loading conditions are reported in Figure 5.

The maximum principal stress at the notch edge of SENB specimens can be evaluated as:

$$\sigma_{p,max} = K\ \sigma_{n,n} \quad \text{for S3PB and NS3PB} \tag{1a}$$

$$\sigma_{p,max} = K\ \tau_{n,n} \qquad \text{for NS4PB} \tag{1b}$$

where $\sigma_{n,n}$ and $\tau_{n,n}$ are the maximum nominal stresses on the net section, evaluated according to the beam theory:

$$\sigma_{n,n} = \frac{6M}{B(W-a)^2} \quad \tau_{n,n} = \frac{3}{2}\frac{Q}{B(W-a)} \tag{2a–b}$$

In Equations (2(a)) and (2(b)), M and Q are the bending moment and the shear force evaluated on the notch bisector resulting from static equilibrium equations:

$$M = F\frac{L_3 - L_1}{L_3 + L_4}L_4 \quad Q = F\left(\frac{L_1}{L_1 + L_2} - \frac{L_3}{L_3 + L_4}\right) \tag{3}$$

Stress concentration coefficients K to be used in Equations (1(a)) and ((b)) have been evaluated by means of finite element analyses and are listed in Table 2.

4. Experimental results

Brittle failure assessments of cracked and blunt notched components are usually based on fracture toughness or strength criteria, respectively. In the former case, according to the fracture mechanics approach, the stress intensity factors (SIFs) at the crack tip are

compared to the fracture toughness of the material. In the latter case, according to classical Notch Theory, the stresses computed in the stress concentration regions are compared to the static strength properties of the material.

In the presence of a blunt notch, namely a notch with a finite value of the root radius ρ, the singularity of the linear elastic crack stress fields disappears. Notwithstanding this, the linear elastic fracture mechanics approach continues to be valid up to a critical value of ρ which varies from material to material according to the following expression [31]:

$$\rho^* = \frac{4}{\pi}\left(\frac{K_{\mathrm{Ic}}}{\sigma_{\mathrm{t}}}\right)^2 \tag{4}$$

For notch root radii greater than the limit value ρ^*, the notch sensitivity is full and the strength of the notched components is controlled by the elastic peak stress value at the notch edge.

A gradual transition between a fracture mechanics-based approach and the peek stress-based approach can be obtained by using local parameters (see, among the others.[32–34])

While discussing the influence of the root radius of crack-like notches on the static fracture load of brittle components, Kullmer and Richard [35] found a relationship similar to that provided by Atzori and Lazzarin [31] for ρ^*, where 4.5 substitutes 4.0.

K_{Ic} and σ_{t} to be used in Equation (4) are the mode I fracture toughness and the critical tensile strength of the material, respectively. While the value of K_{Ic} can be unambiguously determined according to the ASTM-D5045-99 standard,[28,30] particular attention should be paid to the choice of critical material tensile strength. In the literature, indeed, it is suggested to estimate σ_{t} on the basis of the strength of notched components.[34,36,37] In particular, Seweryn [36] suggested that σ_{t} should be determined as 'the maximum normal stress existing at the edge at the moment preceding the cracking' and, to this end, recommended to use tensile specimens with semicircular notches. [37] Thus, according to,[34,36,37] in the present work σ_{t} has been measured evaluating the stress at failure occurring at the tip of DENT specimens. A summary of the obtained σ_{t} values for the neat and nanomodified epoxy resins is shown in Figure 6. It is evident that even if 30B clay-modified epoxy resins exhibit an enhanced fracture toughness,

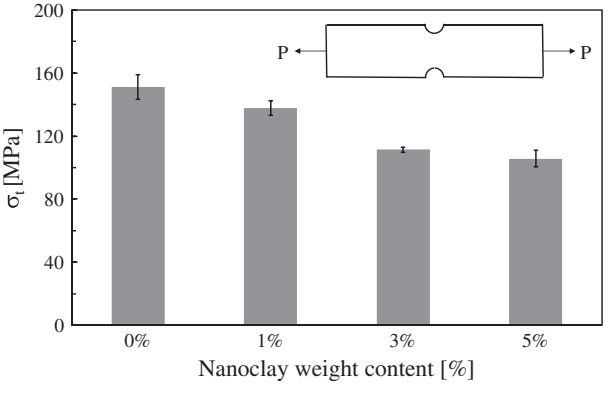

Figure 6. Critical tensile stress, σ_{t}, of the neat and nanomodified epoxy resins (results from DENT tests). Errors bars: ± 2 standard deviations.

[12,26] nanomodification has a detrimental effect on the critical material tensile strength. In more details, σ_t is decreased from about 151 MPa (neat resin) to about 105.7 MPa (5%wt nanoclay) with a reduction of about 30%. This decrease approximately equates that detected, for the same material systems, on the tensile strength as measured from tensile tests on Dog Bone specimens.[12,26]

The limit values for the notch root radius, ρ^*, for the neat resin and the clay-modified resin evaluated by Equation (4) are listed in Table 3. In all cases, ρ^* is smaller than 0.5 mm, namely the smallest value of the notch root radius used in the present analysis, thus indicating that all the specimens analysed in the present work are characterised by a full notch sensitivity.

Accordingly, all experimental data from SENB and DENT specimens with the same nanoclay weight content have been summarised in terms of the maximum principal stress evaluated at the notch edge. The summaries are shown in Figures 7–10, where it is evident that data coming from specimens made of the same material but characterised by different values of the notch root radius and different loading conditions fall within the same narrow scatter band. The scatter bands have been drawn by using for each material configuration the mean values of $\sigma_t \pm 2$ standard deviations.

Thus, for all the notched specimens investigated in this work, nanomodification has a detrimental effect on brittle failure, being it a strength-controlled phenomenon ($\rho > \rho^*$ for all cases). Under these conditions, the disadvantageous role played by nanoclay addition on the strength of polymeric resins [12,14–16] is directly transferred to the notch effect on nanomodified specimens. Accordingly, in the engineering practice, particular care should be taken when using binary nanomodified resins for structural applications in the presence of notches or holes.

Table 3. Fracture toughness, tensile properties and limit notch root radius of neat epoxy and nanomodified polymers.

Clay content %wt	K_{Ic} [MPa $m^{0.5}$] [26]	σ_t [MPa]	a_0 [mm]	ρ^* [mm]
0	1.001 ± 0.024	151.0 ± 3.9	0.013991	0.0559
1	1.489 ± 0.036	137.9 ± 2.33	0.037153	0.1486
3	1.306 ± 0.01	110.8 ± 0.85	0.044274	0.1770
5	1.188 ± 0.034	106.7 ± 2.62	0.039511	0.1580

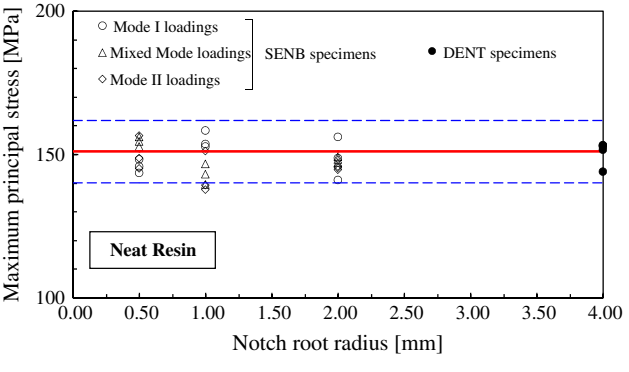

Figure 7. Experimental data from SENB and DENT specimens calculated in terms of the maximum principal stress on the notch edge. Neat resin. Scatter band: mean value ± 2 standard deviations.

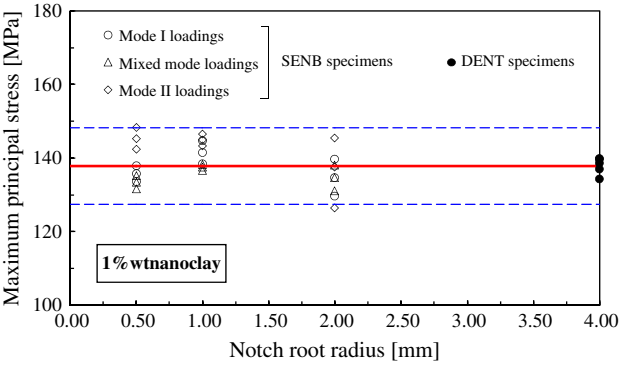

Figure 8. Experimental data from SENB and DENT specimens calculated in terms of the maximum principal stress on the notch edge. 1%wt nanoclay. Scatter band: mean value ± 2 standard deviations.

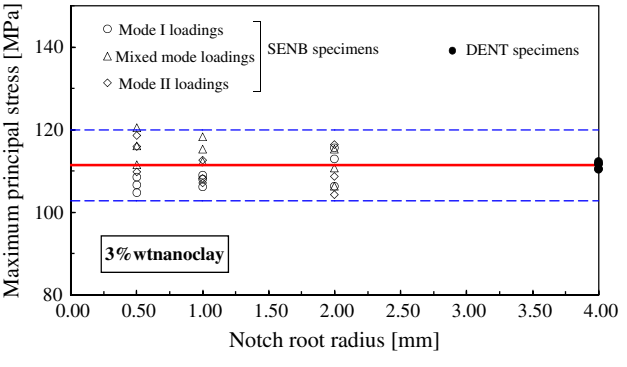

Figure 9. Experimental data from SENB and DENT specimens calculated in terms of the maximum principal stress on the notch edge. 3%wt nanoclay. Scatter band: mean value ± 2 standard deviations.

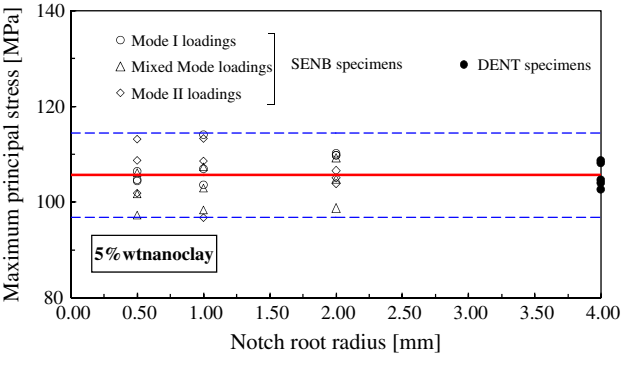

Figure 10. Experimental data from SENB and DENT specimens calculated in terms of the maximum principal stress on the notch edge. 5%wt nanoclay. Scatter band: mean value ± 2 standard deviations.

5. Experimental data in terms of apparent fracture toughness

In this section, the experimental results from SENB specimens already discussed in the previous paragraph will be presented in terms the 'apparent fracture toughness' by using the concept of 'GSIF'.

The SIFs quantify the intensities of the asymptotic linear elastic stress distributions of cracks and are mathematically defined as [38,39]:

$$K_{\mathrm{I}} = \lim_{\mathrm{r}\to 0} \sqrt{2\pi r}\sigma_{\theta\theta} \quad K_{\mathrm{II}} = \lim_{\mathrm{r}\to 0} \sqrt{2\pi r}\tau_{r\theta} \tag{5}$$

When the tip radius is different from zero, the crack becomes a U-notch and the near-the-tip stress field diverges from the singular sharp-crack solution. In this case, Equation (5) should be modified to account for the stress redistribution caused by the presence of a finite value of the notch root radius [40,41]:

$$K_{\mathrm{I}\rho} = \frac{8\sqrt{2\pi r}\,\sigma_{\theta\theta}}{8 + 5\left(\frac{\rho}{r}\right) + 6\left(\frac{\rho}{r}\right)^2 + 5\left(\frac{\rho}{r}\right)^3} \tag{6}$$

$$K_{\mathrm{II}\rho} = \frac{8\sqrt{2\pi r}\,\tau_{\mathrm{r}\theta}}{8 + 13\left(\frac{\rho}{r}\right) - 6\left(\frac{\rho}{r}\right)^2 - 15\left(\frac{\rho}{r}\right)^3} \tag{7}$$

$K_{\mathrm{I}\rho}$ and $K_{\mathrm{II}\rho}$ are commonly regarded as GSIFs. In Equations (6) and (7), r is the distance from the centre of the curvature radius (see Figure 11), ρ is the notch root radius and $\sigma_{\theta\theta}$ and $\tau_{\mathrm{r}\theta}$ are stress components along the notch bisector line to be determined from finite element analyses. It is worth noting that the units of measure of $K_{\mathrm{I}\rho}$ and $K_{\mathrm{II}\rho}$ remain MPa m$^{0.5}$, as for the crack case. Accordingly, unlike the theoretical stress concentration factor K_{t}, the scale effect is fully accounted for by the GSIFs: notched components simply scaled in geometrical proportion have the same K_{t} value, but different GSIF values.

The concept of generalised SIFs, coupled with the cohesive zone model, has been used by Gómez et al. [42] to build a master curve for estimating fracture loads in deep rounded notched components. A generalised equivalent stress intensity fracture, obtained as a generalisation of Glinka's NSIF [43] for mode I simply replacing σ_{tip} by

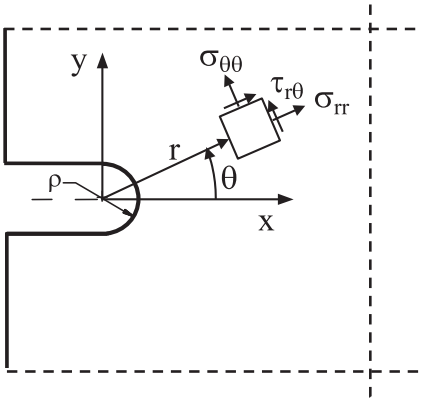

Figure 11. U shaped notch and polar coordinate system to be used in Equations (6) and (7).

the maximum elastic stress at the notch edge, was later used by Gomez et al. [44] to summarise fracture tests from U-notched specimens made of PMMA.

A failure criterion based on the mode I and II GSIFs has also been proposed by Ayatollahi and Torabi and applied to summarise a large number of experimental data from Brazilian disc specimens made of PMMA [45] and polycrystalline graphite.[46] NSIFs have also been recently extended to the elastic-plastic case.[47,48]

The definition or the use of a brittle fracture criterion based on the GSIFs being out of scope of the present research work in this section, GSIFs are used with the only aim to enforce the conclusions drawn in the previous section about the influence of nanomodification on the notch effect on clay-modified epoxy resins. To this end, $K_{I\rho}$ and $K_{II\rho}$ have been evaluated from FE analyses for all SENB specimens and loading conditions considered in the present work, and the experimental results, reconverted in terms of 'apparent fracture toughness', have been summarised in $K_{I\rho}$–$K_{II\rho}$ diagrams (Figures 12–14). It is evident that nanomodified specimens exhibit a lower apparent fracture toughness, independently of the notch root radius. Moreover, differently to what happened for cracked components, where ranging from pure mode I to pure mode II less pronounced improvements of the fracture toughness has been found,[26] no evident effect of the loading mode can be noted here.

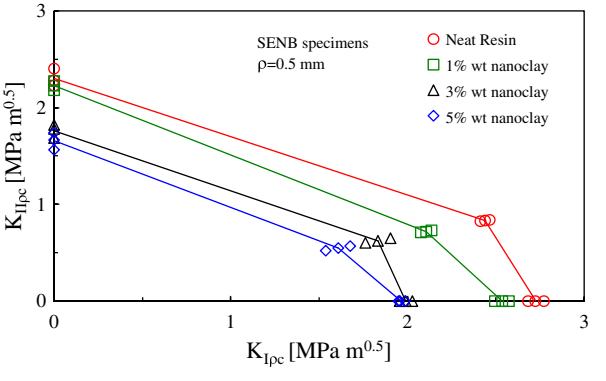

Figure 12. Apparent fracture toughness of neat and nanomodified specimens under various loading conditions. SENB specimens with $\rho = 0.5$ mm.

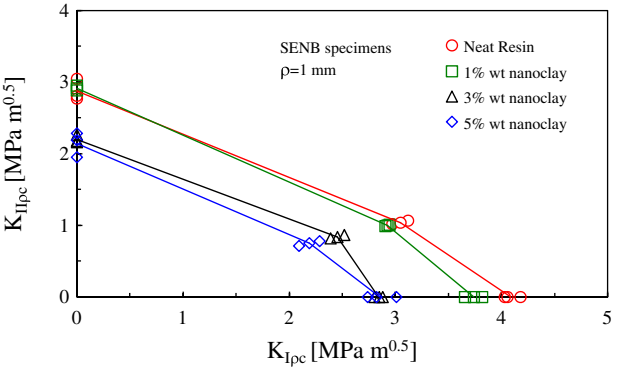

Figure 13. Apparent fracture toughness of neat and nanomodified specimens under various loading conditions. SENB specimens with $\rho = 1$ mm.

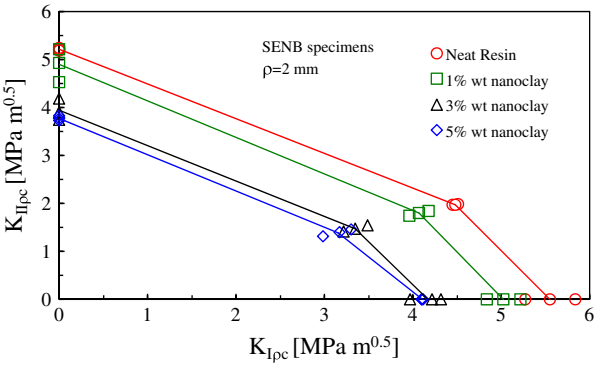

Figure 14. Apparent fracture toughness of neat and nanomodified specimens under various loading conditions. SENB specimens with $\rho = 2$ mm.

6. Conclusion

In the present work, the effects of nanoclay addition on the brittle notch fracture behaviour of an epoxy resin have been studied. Different kind of notched specimens have been manufactured and tested:

(1) DENT specimens with 4 mm radius semicircular notches.
(2) SENB specimens with U-notches. In this case, the notch depth is equal to 10 mm and three different values for the notch root radius have been used: 0.5, 1 and 2 mm.

The experimental results clearly indicate that for notch root radii greater than a limit value, which depends on the clay content, the brittle failure of notched nanomodified components is a strength-controlled phenomenon.

All the results from specimens with the same clay content but with different values of the notch root radius (from 0.5 to 4 mm) were found to be characterised by the same critical value of the maximum principal stress, σ_t. Comparing the average critical values of σ_t allowed us to conclude that for the material systems and geometries investigated in this work, nanomodification has a detrimental effect on the strength of notched components. A final summary of the experimental results in terms of generalised (apparent) fracture toughness revealed that this behaviour is not influenced either by the notch root radius or the loading mode.

As a major conclusion of the present work, it can be stated that, even if nanoclays are suitable to improve the fracture toughness of polymeric systems, the same amelioration is not necessarily transferred to notched parts. Accordingly, in the engineering practice, particular care should be taken when using binary nanomodified resins for structural applications in the presence of notches or holes.

Acknowledgements

The authors greatly acknowledge the financial support to the activity by Veneto Nanotech, the Italian Cluster on Nanotechnologies and by Fondazione Cassa di Risparmio di Padova e Rovigo.

References

[1] Fischer H. Polymer nanocomposites: from fundamental research to specific applications. Mater. Sci. Eng. C. 2003;23:763–772.

[2] Thostenson ET, Li C, Chou TW. Nanocomposites in context. Compos. Sci. Technol. 2005;65:491–516.

[3] Ajayan PM, Schadler LS, Braun PV. Nanocomposite science and technology. Weinheim: Wiley-VCH; 2003.

[4] Zappalorto M, Salviato M, Quaresimin M. A multiscale model to describe nanocomposite fracture toughness enhancement by the plastic yielding of nanovoids. Compos. Sci. Technol. 2012;72:1683–1691.

[5] Salviato M, Zappalorto M, Quaresimin M. Plastic shear bands and fracture toughness improvements of nanoparticle filled polymers: a multiscale analytical model. Composites Part A. 2013;48:144–152.

[6] Zappalorto M, Salviato M, Quaresimin M. Influence of the interphase zone on the nanoparticle debonding stress. Compos. Sci. Technol. 2011;72:48–55.

[7] Sevostianov I, Kachanov M. Effect of interphase layers on the overall elastic and conductive properties of matrix composites. Applications to nanosize inclusion. Int. J. Solids Struct. 2007;44:1304–1315.

[8] Cho JW, Paul DR. Nylon 6 nanocomposites by melt compounding. Polymer. 2001;42:1083–1094.

[9] Wang L, Wang K, Chen L, Zhang Y, He C. Preparation, morphology and thermal/mechanical properties of epoxy/nanoclay composite. Composites Part A. 2006;37:1890–1896.

[10] Liu TX, Liu ZH, Ma KX, Shen L, Zeng KY, He CB. Morphology, thermal and mechanical behavior of polyamide 6/layered-silicate nanocomposites. Compos. Sci. Technol. 2003;63:331–337.

[11] Dorigato A, Pegoretti A, Quaresimin M. Thermo-mechanical characterization of epoxy/clay nanocomposites as matrices for carbon/nanoclay/epoxy laminates. Mater. Sci. Eng. A. 2011;528:6324–6333.

[12] Quaresimin M, Salviato M, Zappalorto M. Fracture and interlaminar properties of clay-modified epoxies and their glass reinforced laminates. Eng. Fract. Mech. 2012;81:80–93.

[13] Lee DC, Jang LW. Preparation and characterization of PMMA-clay hybrid composite by emulsion polymerization. J. Appl. Polym. Sci. 1996;61:1117–1122.

[14] Luo J, Daniel IM. Characterization and modeling of mechanical behavior of polymer/clay nanocomposites. Compos. Sci. Technol. 2003;63:1607–1616.

[15] Bharadwaj RK, Mehrabi AR, Hamilton C, Trujillo C, Murgaa M, Fan R, Chavira A, Thompson AK. Structure-property relationships in cross-linked polyester–clay nanocomposites. Polymer. 2002;43:3699–3705.

[16] Wang K, Chen L, Wu J, Toh ML, He C, Yee AF. Epoxy nanocomposites with highly exfoliated clay: mechanical properties and fracture mechanisms. Macromolecules. 2005;38:788–800.

[17] Quaresimin M, Salviato M, Zappalorto M. Strategies for the assessment of nanocomposite mechanical properties. Composites Part B. 2012;43:2290–2297.

[18] Quaresimin M, Varley RJ. Understanding the effect of nanomodifier addition upon the properties of fibre reinforced laminates. Composites. Sci. Technol. 2008;68:718–726.

[19] Xu Y, Hoa SV. Mechanical properties of carbon fiber reinforced epoxy/clay nanocomposites. Compos. Sci. Technol. 2008;68:854–861.

[20] Subramaniyan AK, Sun CT. Toughening polymeric composites using nanoclay: crack tip scale effects on fracture toughness. Composites Part A. 2007;38:34–43.

[21] Kornmann X, Rees M, Thomann Y, Necola A, Barbezat M, Thomann R. Epoxy-layered silicate nanocomposites as matrix in glass fibre-reinforced composites. Compos. Sci. Technol. 2005;65:2259–2268.

[22] Becker O, Varley R, Simona G. Morphology, thermal relaxations and mechanical properties of layered silicate nanocomposites based upon high-functionality epoxy resins. Polymer. 2002;43:4365–4373.

[23] Liu W, Hoa SV, Pugh M. Fracture toughness and water uptake of high-performance epoxy/nanoclay nanocomposites. Compos. Sci. Technol. 2005;65:2364–2373.

[24] Zerda AS, Lesser AJ. Intercalated clay nanocomposites: morphology, mechanics, and fracture behavior. J. Polym. Sci., Part B: Polym. Phys. 2001;39:1137–1146.

[25] Kornman X, Thomann R, Mulhaupt R, Finter J, Berglund LA. High performance epoxy-layered silicate nanocomposites. Polym. Eng. Sci. 2002;42:1815–1826.
[26] Zappalorto M, Salviato M, Quaresimin M. Mixed mode (I+ II) fracture toughness of polymer nanoclay nanocomposites. Submitted for publication.
[27] Ayatollahi MR, Shadlou S, Shokrieh MM. Mixed mode brittle fracture in epoxy/multi-walled carbon nanotube nanocomposites. Eng. Fract. Mech. 2011;78:2620–2632.
[28] ASTM D 5045. Standard test methods for plane-strain fracture toughness and strain energy release rate of plastic materials. Philadelphia (PA): American Society of Testing and Materials. 1999.
[29] Peterson RE. Stress concentration factors. New York: Wiley; 1974.
[30] Moore DR, Pavan A, Williams JG. Fracture mechanics testing methods for polymers adhesives and composites. Oxford: Elsevier; 2001.
[31] Atzori B, Lazzarin P. Notch sensitivity and defect sensitivity under fatigue loading: two sides of the same medal. Int. J. Fract. 2001;107:L3–L8.
[32] Lazzarin P, Zambardi R. A finite-volume-energy based approach to predict the static and fatigue behaviour of components with sharp V-shaped notches. Int. J. Fract. 2001;112:275–298.
[33] Leguillon D. Strength or toughness? A criterion for crack onset at a notch. Eur. J. Mech. A. Solids. 2002;21:61–72.
[34] Lazzarin P, Berto F. Some expressions for the strain energy in a finite volume surrounding the root of blunt V-notches. Int. J. Fract. 2005;135:161–185.
[35] Kullmer G, Richard HA. Influence of the root radius of crack-like notches on the fracture load of brittle components. Arch. Appl. Mech. 2006;76:711–723.
[36] Seweryn A. Brittle fracture criterion for structures with sharp notches. Eng. Fract. Mech. 1994;47:673–681.
[37] Seweryn A, Lukaszewicz A. Verification of brittle fracture criteria for elements with V-shaped notches. Eng. Fract. Mech. 2002;69:1487–1510.
[38] Irwin GR. Analysis of stresses and strains near the end of a crack traversing a plate. J. Appl. Mech. 1957;24:361–364.
[39] Gross R, Mendelson A. Plane elastostatic analysis of V-notched plates. Int. J. Fract. Mech. 1972;8:267–276.
[40] Zappalorto M, Lazzarin P. In-plane and out-of-plane stress field solutions for V-notches with end holes. Int. J. Fract. 2011;168:167–180.
[41] Lazzarin P, Zappalorto M, Berto F. Generalised stress intensity factors for rounded notches in plates under in-plane shear loading. Int. J. Fract. 2011;170:123–144.
[42] Gómez FJ, Guinea GV, Elices M. Failure criteria for linear elastic materials with U-notches. Int. J. Fract. 2006;141:99–113.
[43] Glinka G. Calculation of inelastic notch-tip strain-stress histories under cyclic loading. Eng. Fract. Mech. 1985;22:839–854.
[44] Gómez FJ, Elices M, Berto F, Lazzarin P. A generalised notch stress intensity factor for U-notched components under mixed mode. Eng. Fract. Mech. 2008;75:4819–4833.
[45] Ayatollahi MR, Torabi AR. Investigation of mixed mode brittle failure in rounded-tip V-notches components. Eng. Fract. Mech. 2010;77:3087–3104.
[46] Ayatollahi MR, Torabi AR. Failure assessment of notched polycrystalline graphite under tensile-shear loading. Mater. Sci. Eng. 2011;528:5685–5695.
[47] Lazzarin P, Zappalorto M. Plastic notch stress intensity factors for pointed V-notches under antiplane shear loading. Int. J. Fract. 2008;152:1–25.
[48] Zappalorto M, Lazzarin P. A new version of the Neuber rule accounting for the influence of the notch opening angle for out-of-plane shear loads. Int. J. Sol. Struct. 2009;46:1901–1910.